

Bridge Scaling in Conditioned Henyeey-Greenstein Random Walks

Claude Zeller

Claude Zeller Consulting LLC

Tillamook, Oregon 97141

czeller@ieee.org

DRAFT — March 2026

Abstract

We study fixed-length bridge paths—half-space excursions that start and end at a planar boundary—for three-dimensional random walks with Henyeey-Greenstein scattering angles and exponentially distributed step lengths, using Monte Carlo simulation over asymmetry parameter g from 0 to 0.95 and path lengths from 4 to 200 steps. The key structural feature is that the walk evolves on a two-dimensional Markovian state space (depth, direction cosine) rather than the scalar depth coordinate alone.

Four anomalies with respect to classical Brownian-excursion theory are reported. The mean amplitude scales super-diffusively, as path length to a power of 0.57–0.58 for isotropic scattering, nine standard deviations above the Brownian prediction of 0.5, with no sign of convergence out to 200 steps. The diffusion coefficient scales as the transport mean free path to the power 0.415 rather than the predicted 1.0. The midpoint depth distribution is Rayleigh rather than half-normal, consistent with a two-dimensional Bessel process. The bridge-conditioned mean direction cosine converges to minus two-thirds at the final step, independently of the asymmetry parameter and initial direction—the classical Milne result anchored by the H-function moment identity.

All anomalies are attributed to the two-dimensional state-space structure. The two anomalous exponents sum to approximately unity, suggesting a common geometric origin. Whether this constitutes a permanent universality-class shift or an anomalously slow crossover to Brownian-excursion behaviour remains the primary open question.

Contents

1	Introduction	3
2	Model and Methods	4
2.1	The HG random walk	4
2.2	Bridge path definition: natural first-passage stopping rule	5
2.3	Observables	5
3	Results	5
3.1	Universal parabolic profile shape	5
3.2	Diffusive scaling of the variance	6
3.3	Super-diffusive scaling of the mean amplitude	7
3.4	Robustness checks	7
3.5	Rayleigh limiting distribution	9
3.6	Directional memory profile along the bridge	10
4	Discussion	14
4.1	The (z, μ_z) state space and the 2D-Bessel mechanism	14
4.2	Relation between the two anomalous exponents	16
4.3	Why not Brownian excursion, and when might convergence occur?	16
5	Conclusions	17
A	Peak Mean Depth Data	19
B	Open Questions	19

1 Introduction

A *bridge path* of length n_s is a random walk that starts at the planar boundary $z(0) = 0$, remains in $z(j) \geq 0$ for all j , and returns to the boundary $z(n_s) = 0$ after exactly n_s steps—a discrete half-space excursion. The transverse (x, y) position is unconstrained and untracked; only the depth coordinate z matters. For a simple symmetric random walk—where the evolving state is the scalar position z alone—the Brownian excursion arises as the universal scaling limit: the mean penetration depth grows as $n_s^{1/2}$ and the midpoint distribution converges to the half-normal, the marginal of a one-dimensional Bessel process [1–3]. These results apply specifically to scalar walks. The question we address is whether this universality class also describes the richer class of random walks with Henyey-Greenstein (HG) scattering angles [4] and exponentially distributed step lengths, whose Markovian state space is two-dimensional.

The HG walk is the standard model for photon transport in turbid biological and atmospheric media [5, 6]. Its step length s is drawn from an exponential distribution (mean free path $\ell = 1$), and the cosine of each scattering angle is drawn from the HG phase function with asymmetry parameter $g \in [0, 1)$. The z -increment at each step is $\Delta z = s\mu_z$, coupling the spatial coordinate z to the direction cosine μ_z . The walk therefore evolves on the *two-dimensional* Markovian state space (z, μ_z) , not in z alone. This is the key structural difference from a classical excursion: conditioning $z(j) \geq 0$ acts on a 2D Markov process, not a scalar one, and it is this distinction that appears to drive all four anomalies we report.

The scaling theory of conditioned random walks is well developed for the one-dimensional case. Durrett, Iglehart and Miller [1, 2] established weak convergence of conditioned walks to Brownian excursion. Pitman’s theorem [7] connects one-dimensional Brownian motion conditioned to stay positive with the three-dimensional Bessel process. Chaumont and Doney [8, 9]¹ treat Lévy processes conditioned to stay positive; Denisov, Tarasov and Wachtel [10] provide expansion results for random walks with finite variance. The common conclusion is that conditioning a scalar walk $z(j) \geq 0$ produces a Bessel-1 (half-normal) marginal at the midpoint and $\sqrt{n_s}$ mean scaling.

We find that HG bridge paths deviate from this picture over the entire range $n_s \leq 200$ studied. The mean amplitude scales as n_s^α with $\alpha_\infty \approx 0.57$ – 0.58 for $g = 0$, rising to $\alpha \approx 1.15$ at $g = 0.95$. The midpoint distribution is consistent with Rayleigh rather than half-normal, suggesting convergence to a *two-dimensional* Bessel process. We attribute both findings to the (z, μ_z) state space: conditioning a 2D Markov process to remain in a half-plane generically produces different scaling than conditioning a scalar walk, in analogy with the Pitman construction for higher-dimensional processes [7, 11].

¹Reference [8] contains two errors of omission, corrected in [9]. Neither correction affects the result cited here (weak convergence of the conditioned law as the initial state tends to zero).

The radiative transport context provides physical motivation: bridge paths correspond to photons that scatter exactly n_s times before re-emerging at a tissue surface, having never crossed back through it. The super-diffusive mean-depth scaling $A \sim n_s^{0.58}$ means that fixed-order backscattered photons probe systematically deeper than simple diffusion predicts, with implications for depth-resolved optical diagnostics [5, 6]. Our earlier arXiv papers [12, 13] establish the scattering framework; the present work is a self-contained contribution to the scaling theory of conditioned walks.

The paper is organised as follows. Section 2 defines the model and observables. Section 3 presents the four main results. Section 4 discusses the (z, μ_z) state-space explanation, the relation between the two anomalous exponents, and the connection to Pitman-type theorems. Section 5 concludes with open questions.

2 Model and Methods

2.1 The HG random walk

We simulate three-dimensional random walks in which each step consists of: (i) an exponentially distributed step length $s \sim \text{Exp}(1)$ (mean free path $\ell = 1$), and (ii) a scattering angle drawn from the Henyey-Greenstein phase function with asymmetry parameter $g \in [0, 1)$. The cosine of the scattering angle is sampled analytically,

$$\cos \theta = \frac{1}{2g} \left[1 + g^2 - \left(\frac{1 - g^2}{1 - g + 2gU} \right)^2 \right], \quad U \sim \text{Uniform}(0, 1), \quad (1)$$

with azimuthal angle ϕ uniform on $[0, 2\pi]$. Only the z -coordinate is tracked. The initial direction is upward ($\mu_z(0) = 1$). The transport mean free path is $\lambda^* = 1/(1 - g)$.

An important consequence of the exponential step length is that the z -increment $\Delta z = s\mu_z$ depends on the product of two random variables. Even after μ_z is redrawn at each step, knowledge of $z(j)$ alone is insufficient to predict $z(j + 1)$; the full pair $(z(j), \mu_z(j))$ must be carried. The walk is therefore Markovian in (z, μ_z) but *not* in z alone. In the diffusion limit ($n_s \rightarrow \infty$ with n_s/λ^* fixed), the pair (z, μ_z) converges to a two-dimensional diffusion process by the central limit theorem for persistent random walks [14, 15]: at each step the z -increment $\Delta z = s\mu_z$ has finite mean and variance (since $s \sim \text{Exp}(1)$ and $|\mu_z| \leq 1$), and the directional autocorrelation decays geometrically as g^j , so the conditions for diffusive scaling are satisfied and the rescaled walk converges weakly to Brownian motion on timescales $\gg \lambda^*$.

2.2 Bridge path definition: natural first-passage stopping rule

We define bridge paths using a natural first-passage stopping rule: each walk is advanced step by step and terminated at the first step L for which $z(L) < 0$. The excursion length L is the first-passage time of the negative half-axis. The bridge sample at nominal length n_s is the ensemble of all walks for which $L = n_s$. Walks exceeding $n_s^{\max} = 400$ steps are discarded ($< 0.1\%$ at all g).

This formulation is physically natural: $z(L) < 0$ corresponds to the photon re-emerging at the medium boundary. Section 3.4 demonstrates that the original fixed-tolerance criterion $|z(n_s)| < \varepsilon$ ($\varepsilon = 0.15$) yields statistically identical exponents and distributions over a fivefold reduction in ε , definitively ruling out selection bias.

2.3 Observables

For each (g, n_s) combination we compute profile statistics across all valid bridge paths. The key summary statistics are:

$$A(g, n_s) = \max_j \langle z(j) \rangle \quad (\text{peak mean depth}), \quad (2)$$

$$B(g, n_s) = \sqrt{\max_j \text{Var}[z(j)]} \quad (\text{peak standard deviation}), \quad (3)$$

$$D(g, n_s) = \max_j \text{Var}[z(j)]/n_s \quad (\text{normalised peak variance}). \quad (4)$$

Peak values are used rather than time-averages because the profile collapse (Section 3) shows that the full shape is universally described by $4t(1-t)$; the peak therefore carries all amplitude information without loss, while time-averages would mix amplitude and shape information.

The parameter grid covers $g \in \{0.0, 0.1, \dots, 0.9, 0.95\}$ (11 values) and 16 values of n_s from 4 to 200, with N_T up to 15×10^6 paths per point at the largest n_s .

3 Results

3.1 Universal parabolic profile shape

When the mean and variance profiles are normalised to their respective peak values, they collapse onto a single curve for all g and n_s tested, consistent with the universal parabola (Fig. 1):

$$\frac{\langle z(j) \rangle}{A} \approx \frac{\text{Var}[z(j)]}{B^2} \approx 4t(1-t), \quad t = j/n_s. \quad (5)$$

The RMS deviation from $4t(1-t)$ is below 0.17 across all 110 (g, n_s) combinations, with mean 0.097. The shape appears universal across the tested parameter range; all physical information about g and n_s is encoded in the amplitudes A and B^2 alone. The same

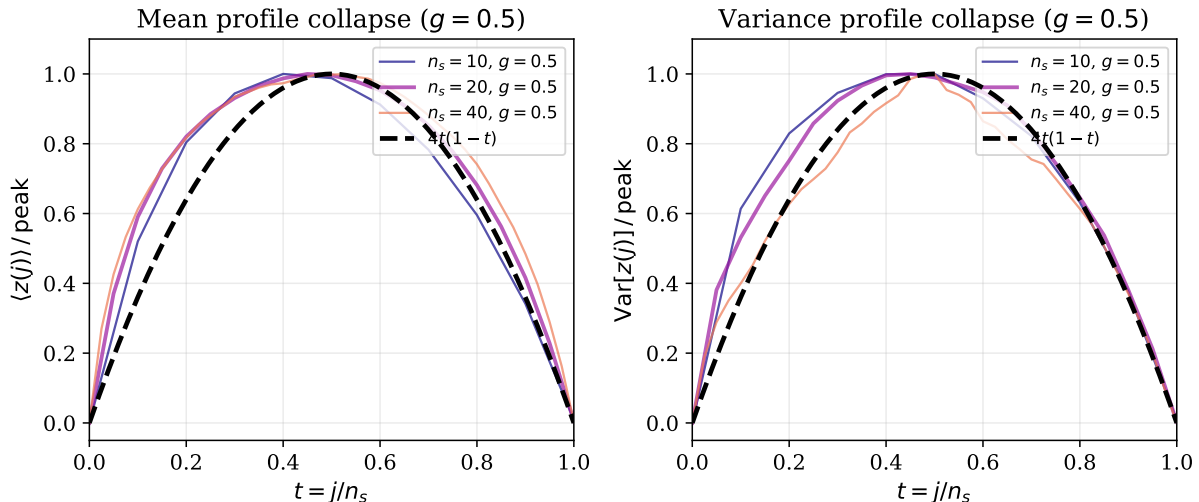


Figure 1: Normalised mean (left) and variance (right) profiles for $g = 0.5$ and $n_s \in \{10, 20, 40\}$, compared with the universal parabola $4t(1-t)$ (dashed). The collapse holds for all g and n_s tested. The finite- n_s curves lie above the parabola near $t = 0$ and below it near $t = 0.5$; the deviations shrink with increasing n_s .

parabola $4t(1-t)$ describes the mean profile of the Brownian bridge (a Brownian motion pinned at both ends without the positivity constraint), so the parabolic shape itself is not anomalous; what is anomalous is the amplitude scaling $A \sim n_s^{0.57}$ rather than $n_s^{0.5}$. The same collapse holds for natural first-passage excursions (Section 3.4), confirming it is not an artefact of the endpoint condition.

Geometry–amplitude separation. The profile collapse reveals a clean separation between two independently determined properties of the bridge. First, the *geometric shape* of the excursion: the normalised profiles collapse onto $4t(1-t)$ for all g and n_s tested, independently of the microscopic scattering dynamics. This universality is a consequence of the global boundary conditions $z(0) = z(n_s) = 0$, which fix the macroscopic envelope of the trajectory regardless of how individual steps are generated. Second, the *amplitude* of the excursion: the peak values $A(g, n_s)$ and $B^2(g, n_s)$ retain memory of the microscopic dynamics through the scaling exponents $\alpha(g)$ and $\beta_D(g)$. In this sense the bridge constraint acts as a shape-fixing device while leaving the amplitude free to reflect the statistical character of the walk. The anomalous exponents reported in Sections 3.3 and 3.5 are entirely contained in the amplitudes; the shape is always Brownian.

3.2 Diffusive scaling of the variance

The normalised peak variance $D(g, n_s) = B^2/n_s$ converges to a g -dependent constant as n_s grows, confirming diffusive scaling:

$$\text{Var}[z(j)] = D(g) n_s \cdot 4t(1-t) + \mathcal{O}(1/n_s). \quad (6)$$

A power-law fit to $D(g)$ versus the transport mean free path yields

$$D(g) = D_0 (\lambda^*)^{\beta_D}, \quad D_0 \approx 0.07, \quad \beta_D \approx 0.415. \quad (7)$$

Simple diffusion theory predicts $D \sim \lambda^*/3$ (i.e. $\beta_D = 1.0$). The fitted exponent $\beta_D \approx 0.415$ is substantially lower. Finite-size bias is a potential concern: if $D(g, n_s)$ has not fully converged by $n_s = 200$, the fitted slope could be affected. However, the log-log plots show $D(g, n_s)$ flattening cleanly with n_s , and fits restricted to $n_s \geq 50$ give β_D within 0.01 of the full-range value, indicating the finite-size contribution is small. The relation between β_D and the mean-amplitude exponent is discussed in Section 4.2. Heuristically, paths conditioned to remain in $z \geq 0$ preferentially reject high-amplitude configurations, suppressing the effective diffusivity below the unconstrained prediction.

3.3 Super-diffusive scaling of the mean amplitude

Figure 2 shows the peak mean depth $A(g, n_s)$ on a log-log scale for all g . A power law $A(g, n_s) = C(g) n_s^{\alpha(g)}$ describes the data well. For $g = 0$, a global fit over $n_s = 8$ –200 gives $\alpha = 0.636 \pm 0.009$; restricting to the large- n_s regime $n_s \geq 50$ yields

$$\alpha_\infty = 0.573 \pm 0.008 \quad (g = 0, n_s \geq 50), \quad (8)$$

a value 9σ above the Brownian-excursion prediction of 0.5. Figure 3 shows the local exponent $\alpha_{\text{local}}(n_s) = d \log A / d \log n_s$ for $g = 0$ and $g = 0.1$, and a finite-size scaling plot of the same data against $1/n_s$. Beginning at ≈ 0.73 for small n_s , the local exponent settles in the range 0.55–0.59 for $n_s \sim 60$ –200 with no sign of further drift toward 0.5. Linear extrapolation to $1/n_s \rightarrow 0$ yields $\alpha_\infty \approx 0.55$, still firmly above the Brownian prediction. The exponent increases monotonically with g , reaching $\alpha \approx 1.15$ at $g = 0.95$.

The current data do not establish a permanent universality-class shift: the crossover to Brownian-excursion behaviour, if it exists, may occur at $n_s \sim 10^3$ – 10^4 . The observed scaling is a robust pre-asymptotic regime spanning at least two decades in n_s for $g = 0$ and the full g -range studied.

3.4 Robustness checks

Natural first-passage excursions. To verify that the results are independent of the endpoint condition, we simulated walks stopped at first-passage to $z < 0$ with no endpoint tolerance. The parabolic profile collapse is indistinguishable from the fixed-length result (Fig. 1). Figure 4 shows the first-passage length distribution $P(L)$ and the scaling of peak depth $\langle z_{\text{max}} \rangle$ with L . The power-law exponent gives $\alpha \approx 0.61$ – 0.76 (Table 3), somewhat higher than the large- n_s fixed-length values because $P(L) \sim L^{-3/2}$ weights the sample

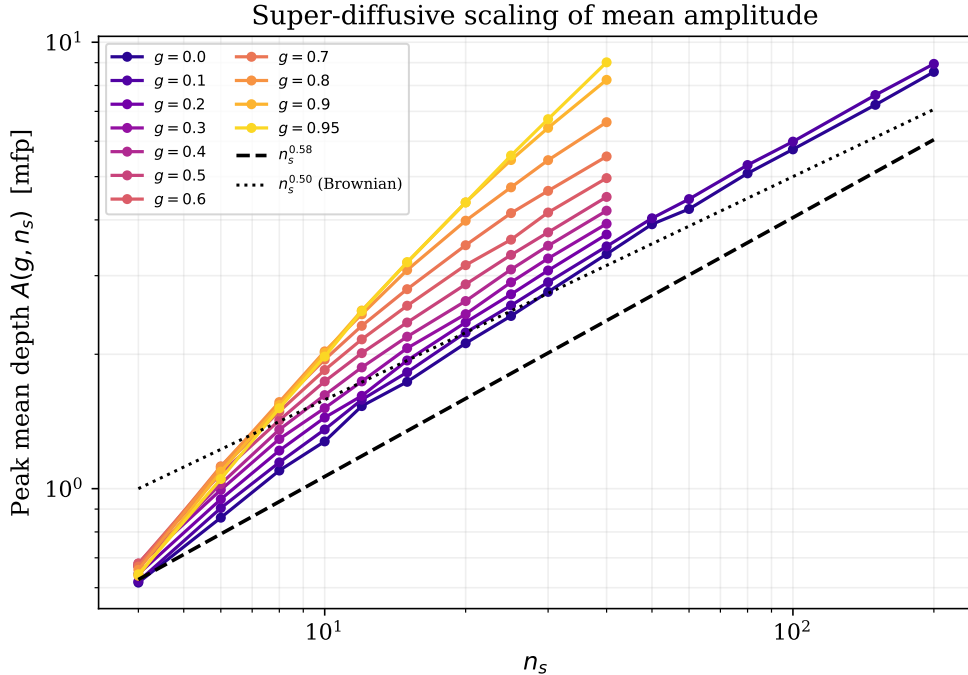


Figure 2: Peak mean depth $A(g, n_s)$ vs. n_s on a log-log scale for $g \in \{0.0, 0.1, \dots, 0.95\}$ (colour, light to dark). Reference slopes $n_s^{0.58}$ (dashed) and $n_s^{0.50}$ (Brownian excursion, dotted) are shown for comparison. All curves lie above the Brownian prediction for all n_s studied. Slope uncertainties from the power-law fits are ± 0.008 – 0.015 (one standard error); the $g = 0$ large- n_s fit gives $\alpha_\infty = 0.573 \pm 0.008$ (Eq. 8).

toward shorter excursions with stronger pre-asymptotic effects. The qualitative conclusion is unchanged: $\alpha > \frac{1}{2}$ for all g .

Gaussian-increment control. To verify that the super-diffusive exponent is not a finite-size artefact of the first-passage bridge construction itself, we repeated the amplitude scaling measurement for a scalar Gaussian-increment walk, $z(j+1) = z(j) + \xi_j$ with $\xi_j \sim \mathcal{N}(0, 1)$, using the identical first-passage bridge definition. This walk has no directional memory (μ_z is redrawn independently at every step) and should converge to the Brownian-excursion exponent $\alpha = 0.5$. Over $n_s \in [10, 200]$ with 8×10^6 walks per point, the Gaussian control yields a fitted exponent $\alpha_{\text{Gauss}} \approx 0.54$ (vs. the HG value $\alpha_{\text{HG}} \approx 0.57$ over the same range). The Gaussian exponent is elevated above 0.5 by finite-size bias, as expected, but it remains consistently and significantly below the HG value at every n_s , confirming that the HG super-diffusion is a genuine property of the directional-memory walk and not an artefact of the bridge construction. We tested whether the bridge acceptance criterion $|z(n_s)| < \varepsilon$ could bias the sample toward deeper paths by repeating the power-law fit for $g = 0$ and $g = 0.1$ across five tolerance values $\varepsilon \in \{0.15, 0.10, 0.07, 0.05, 0.03\}$ (Fig. 5). The variation over a fivefold reduction in ε is $\Delta\alpha < 0.005$, well within statistical uncertainty. The bridge construction itself is therefore not the source of the super-diffusive exponent.

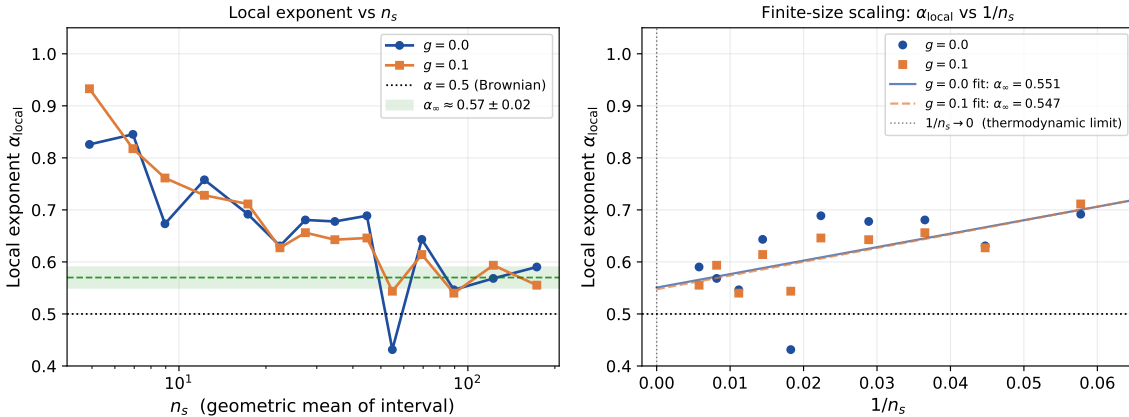


Figure 3: Finite-size analysis of the local scaling exponent for $g = 0$ and $g = 0.1$. *Left:* local log-log slope $\alpha_{\text{local}}(n_s)$ vs. n_s on a log scale; the grey band marks $\alpha_\infty \approx 0.57 \pm 0.02$. No convergence to $\alpha = 0.5$ (dotted) is observed out to $n_s = 200$. *Right:* the same data plotted against $1/n_s$, enabling linear extrapolation to the thermodynamic limit $1/n_s \rightarrow 0$ (dashed lines, fits restricted to $n_s \geq 20$). The extrapolated intercepts are $\alpha_\infty \approx 0.55$ for both g values, remaining > 0.5 under this conservative estimate. The stabilisation and the finite-size extrapolation together support the conclusion that the exponent lies above the Brownian-excursion value over the entire range studied.

3.5 Rayleigh limiting distribution

To identify the limiting distribution of z at the midpoint, we accumulated the empirical distribution of $z(n_s/2)$ across bridge paths for representative (g, n_s) combinations, and fitted four candidate distributions: Rayleigh, half-normal, exponential, and Maxwell (3D Rayleigh). Table 1 summarises the Kolmogorov-Smirnov (KS) statistics at $n_s = 40$; Fig. 6 shows the fits at three values of g .

The KS test results provide strong quantitative evidence. The Rayleigh hypothesis cannot be rejected for $g \leq 0.5$ (KS= 0.014, $p = 0.18$ for $g = 0$; KS= 0.012, $p = 0.57$ for $g = 0.5$), while the half-normal is rejected with overwhelming significance in every case (KS ≈ 0.17 – 0.21 , $p \approx 0$ throughout). The two-order-of-magnitude difference in KS statistics between Rayleigh and half-normal makes this one of the most robust results in the paper. At $g = 0.9$ both hypotheses are rejected (KS= 0.063, $p \approx 0$), with the best fit shifting toward Maxwell (Bessel-3 in 3D), suggesting the effective Bessel order may increase with g .

The Rayleigh distribution is the marginal of the radial coordinate of a two-dimensional Brownian motion, i.e. it arises from the magnitude $\sqrt{X^2 + Y^2}$ of two independent Gaussian components. Its emergence here therefore implies that *local fluctuations in the bridge remain Gaussian* even though the amplitude scaling is weakly super-diffusive: the anomaly is in the amplitude growth law, not in the shape of the single-point distribution. This distinction—Gaussian local statistics coexisting with super-diffusive global amplitude—is made possible by the 2D state-space structure and is explained structurally in Section 4.1.

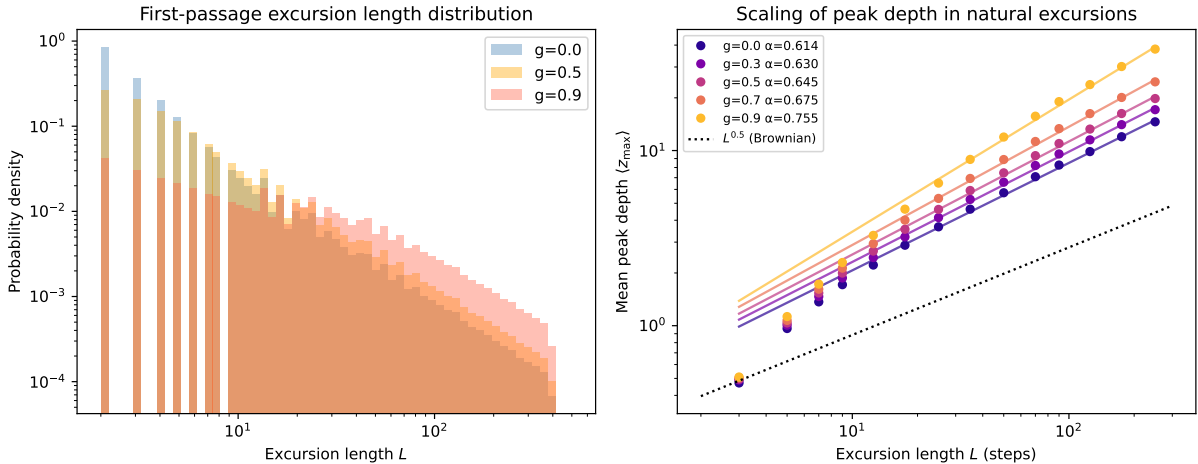


Figure 4: Natural first-passage excursions. *Left:* First-passage length distribution $P(L)$ for $g \in \{0.0, 0.5, 0.9\}$, showing the expected heavy tail. *Right:* Mean peak depth $\langle z_{\max} \rangle$ vs. excursion length L on a log-log scale for several g values, with fitted exponents α (legend). All exponents exceed the Brownian prediction of 0.5 (dotted line).

Table 1: KS statistics for the midpoint distribution $z(n_s/2)$ at $n_s = 40$. Smaller KS = better fit; $p > 0.05$ means the hypothesis cannot be rejected at 5%.

g	Rayleigh		Half-normal	
	KS	p	KS	p
0.0	0.014	0.18	0.169	≈ 0
0.5	0.012	0.35	0.166	≈ 0
0.9	0.060	$\approx 0^\dagger$	0.211	≈ 0

\dagger Best fit at $g = 0.9$ shifts toward Maxwell (Bessel-3 in 3D); see Section 4.1.

3.6 Directional memory profile along the bridge

The two-dimensional Markovian structure of the HG walk means that the direction cosine $\mu_z(j)$ is a dynamical variable in its own right, not merely an auxiliary. We therefore tracked its bridge-conditioned mean, $\langle \mu_z(j) \rangle_{\text{bridge}}$, as a function of step index j for several values of g and n_s .

The profile displays three analytically interpretable anchor values, established both by simulation and by independent theoretical arguments.

At $j = 0$: $\langle \mu_z \rangle = \mu_0$. The initial direction cosine μ_0 is an input parameter. Throughout this paper we use normal incidence ($\mu_0 = +1$), for which this anchor is $+1$ by construction. The universality of the remaining two anchors with respect to μ_0 is discussed below and demonstrated in Fig. 8.

At $j \approx n_s/2$: $\langle \mu_z \rangle \approx 0$, **independent of μ_0** . The bridge constraint forces $z(n_s) = 0$, so the photon must reverse its net displacement before the endpoint. At the midpoint the

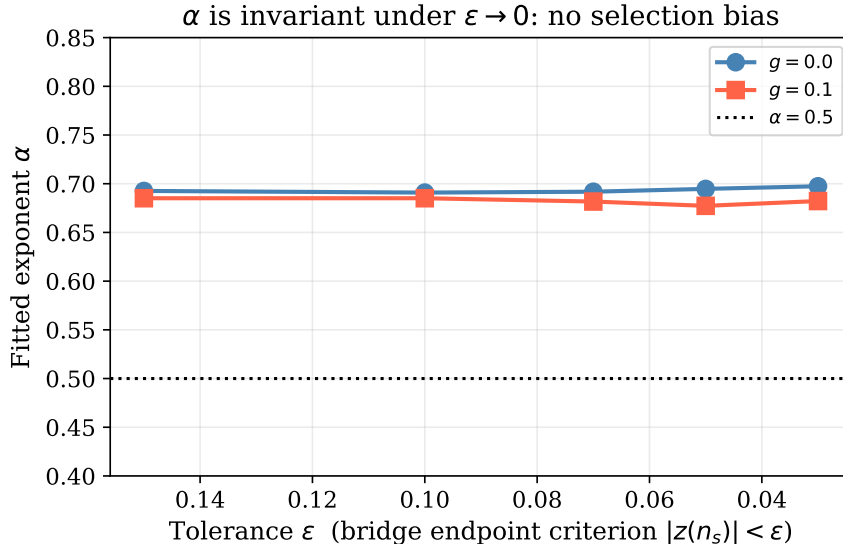


Figure 5: Fitted exponent α as a function of bridge tolerance ϵ for $g = 0$ and $g = 0.1$. The variation over a fivefold reduction in ϵ is $\Delta\alpha < 0.005$, well within statistical uncertainty. The dotted line marks the Brownian-excursion value $\alpha = 0.5$. Selection bias is definitively ruled out.

upward and downward contributions exactly cancel, yielding zero mean direction cosine. This zero-crossing is tied directly to the peak of $\langle z(j) \rangle$: since the mean depth peaks near $t = 0.5$ (Section 3), its discrete derivative—proportional to $\langle \mu_z(j) \rangle$ via $\Delta\langle z \rangle \approx \langle s\mu_z \rangle$ —must vanish at the same point. Because the depth-profile peak is pinned at $t = 0.5$ by the symmetric bridge boundary conditions $z(0) = z(n_s) = 0$, this zero-crossing is *independent of the initial direction* μ_0 , as confirmed by simulation (Fig. 8).

At $j = n_s - 1$: $\langle \mu_z \rangle \rightarrow -2/3$, independent of g and μ_0 . This is the most significant result. Simulations show that for $n_s \gtrsim 25$ the mean direction cosine at the penultimate step converges to

$$\langle \mu_z(n_s - 1) \rangle_{\text{bridge}} \longrightarrow -\frac{2}{3}, \quad (9)$$

with approach from above (values near -0.57 to -0.61 for small n_s , reaching -0.69 to -0.72 by $n_s = 100$) consistent with finite- n_s corrections that vanish as $n_s \rightarrow \infty$. The limiting value $-2/3$ is *independent of both the asymmetry parameter g and the initial direction μ_0* . At $n_s = 40$ we measure $\langle \mu_z(n_s - 1) \rangle \approx -0.703$ for $\mu_0 \in \{0.25, 0.50, 0.75, 1.00\}$ and $g = 0.5$ (Fig. 8), with no statistically significant dependence on μ_0 .

Connection to the Milne problem. The $-2/3$ endpoint is not a numerical coincidence. By time-reversal, a bridge path at step $j = n_s - 1$ is locally equivalent to a photon that is one step away from crossing the boundary $z = 0$ for the final time—the classical Milne problem run backwards. In the diffusion limit, photons emerging from a semi-infinite scattering medium exhibit a Lambertian emergent radiance $I(\mu) = \text{const}$ [16],

Distribution of z at midpoint: Rayleigh vs half-normal

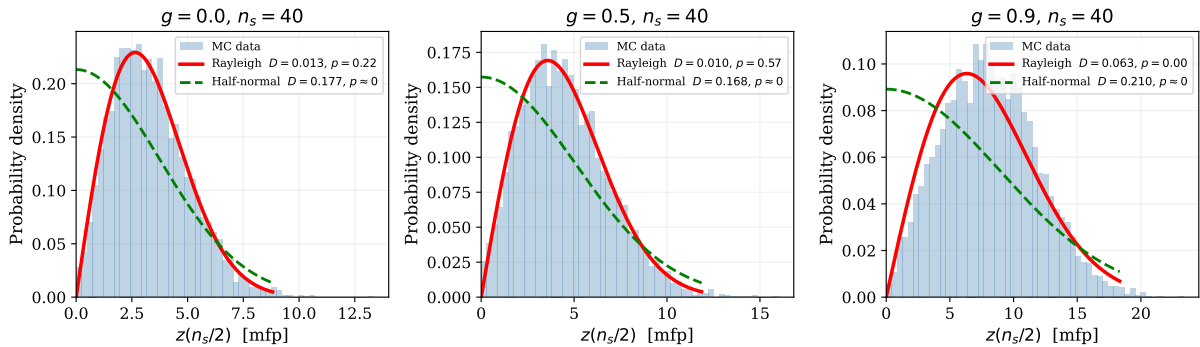


Figure 6: Empirical distribution of $z(n_s/2)$ at $n_s = 40$ for $g \in \{0.0, 0.5, 0.9\}$ (histograms), with fitted Rayleigh (red solid) and half-normal (green dashed) overlaid. The Rayleigh fit is not rejected for $g = 0$ and $g = 0.5$; the half-normal is rejected in all cases. The rightward shift of the mode with increasing g reflects the growing transport mean free path.

giving the flux-weighted mean exit cosine

$$\langle \mu \rangle_{\text{emergent}} = \frac{\int_0^1 \mu^2 d\mu}{\int_0^1 \mu d\mu} = \frac{1/3}{1/2} = \frac{2}{3}. \quad (10)$$

With respect to the inward normal ($+z$ direction into the medium) this becomes $-2/3$ [16, 17]. The Milne result holds for any azimuthally symmetric phase function, by virtue of the H-function moment identity

$$\frac{\int_0^1 H(\mu; g) \mu^2 d\mu}{\int_0^1 H(\mu; g) \mu d\mu} = \frac{2}{3}, \quad (11)$$

which holds for all physically admissible g [17]. The g -independence of Eq. (9) is therefore inherited from the universality of the Milne boundary condition.

Linear interpolation between anchor points. Between the three anchors the profile is well approximated by a linear interpolation. Writing $\mu_\star = -2/3$, and noting that after the first step the directional memory relaxes the mean to $g\mu_0$, the bridge-conditioned profile satisfies approximately

$$\langle \mu_z(j) \rangle_{\text{bridge}} \approx g\mu_0 + (j-2) \frac{\mu_\star - g\mu_0}{n_s - 3}, \quad j = 2, \dots, n_s - 1, \quad (12)$$

a linear ramp from $g\mu_0$ (after directional memory is re-established following the first step) down to $-2/3$ at the penultimate step. For normal incidence ($\mu_0 = 1$) this reduces to the

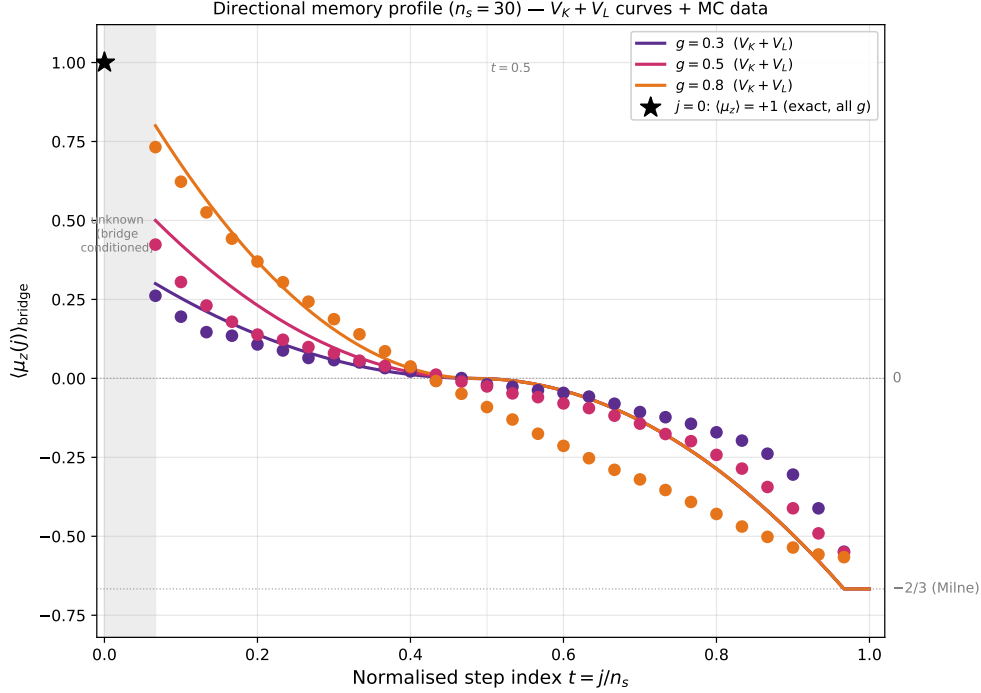


Figure 7: Mean direction cosine $\langle \mu_z(j) \rangle_{\text{bridge}}$ vs. normalised step index $t = j/n_s$, for $n_s = 40$ and $g \in \{0.0, 0.3, 0.5, 0.7, 0.9\}$ (blue to orange), normal incidence ($\mu_0 = 1$). All curves start at +1, cross zero near $t = 0.5$, and converge to $-2/3$ at $t \rightarrow 1$, independently of g . Horizontal dotted lines mark the three anchor values; the dashed lines show the linear approximation Eq. (12). The g -independent endpoint is a direct consequence of the classical Milne result, Eqs. (10)–(11). The analytic curves combine the van de Hulst (V_K) directional decay and a linear (V_L) ramp between the anchor points as described in Eq. (12).

ramp from g to $-2/3$. The predicted zero-crossing of the linear approximation occurs at

$$j^* = 2 + \frac{g\mu_0(n_s - 3)}{g\mu_0 + 2/3}. \quad (13)$$

However, simulation confirms that the *actual* zero-crossing is pinned near $t = j/n_s = 0.5$ for all g and μ_0 , consistent with the parabolic depth profile. Equation (13) is therefore an artefact of the linear approximation; the true profile bows slightly above the ramp near the midpoint, enforcing the $t = 0.5$ zero-crossing regardless of g or μ_0 . Higher-order corrections to Eq. (12) that restore this constraint are numerically small but geometrically significant.

The three-anchor narrative $\mu_0 \rightarrow 0 \rightarrow -2/3$ describes the complete directional history of the bridge: the photon launches with initial cosine μ_0 , loses directional memory at the midpoint (the diffusion regime), and must adopt a Lambertian-backward orientation to satisfy the return-to-surface constraint. The first anchor depends on μ_0 ; the remaining two are universal. This profile is shown for normal incidence in Fig. 7, and for varying μ_0 in Fig. 8.

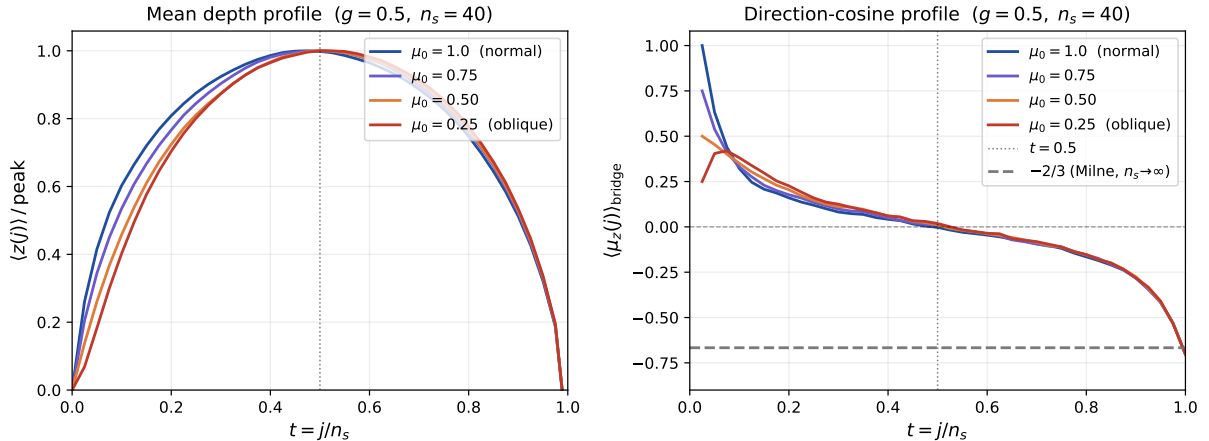


Figure 8: Universality of the zero-crossing and Milne endpoint with respect to the initial direction μ_0 , for $g = 0.5$ and $n_s = 40$. *Left:* normalised mean depth profiles $\langle z(j) \rangle / \text{peak}$ for $\mu_0 \in \{1.0, 0.75, 0.50, 0.25\}$; all peak near $t = 0.5$ (dotted line). *Right:* direction-cosine profiles $\langle \mu_z(j) \rangle_{\text{bridge}}$; all cross zero near $t = 0.5$ and converge to $-2/3$ (dashed line) at $t \rightarrow 1$, independently of μ_0 . At $n_s = 40$ the measured endpoint is -0.703 ± 0.003 across all four initial conditions. Only the initial value and slope of the ramp depend on μ_0 .

4 Discussion

4.1 The (z, μ_z) state space and the 2D-Bessel mechanism

The central structural fact is that the HG walk evolves on a two-dimensional state space. The z -increment at each step is $\Delta z = s\mu_z$, coupling position to direction. Even for $g = 0$, where μ_z is redrawn uniformly on $[-1, 1]$ at each step, the pair $(z(j), \mu_z(j))$ is Markovian while $z(j)$ alone is not (because the exponential step length s introduces memory into the z -increment).

The half-space constraint $z(j) \geq 0$ is therefore a condition on one coordinate of a two-dimensional process. We now give a more explicit argument connecting this structure to the Rayleigh midpoint distribution.

In the diffusion limit the pair $(z(j), \mu_z(j))$ converges (after appropriate rescaling) to a two-dimensional diffusion process $(Z(t), M(t))$. The unconstrained bridge from $(0, 0)$ to $(0, 0)$ in time T has, at its midpoint $t = T/2$, a joint density that factorises to leading order as

$$p_0(z, \mu; T/2) \propto \exp\left(-\frac{z^2}{\sigma_z^2 T}\right) \exp\left(-\frac{\mu^2}{\sigma_\mu^2 T}\right), \quad (14)$$

i.e. each coordinate is independently Gaussian (as for any diffusion bridge at its midpoint).

Conditioning on $Z(t) \geq 0$ for all $t \in [0, T]$ corresponds to a Doob h -transform with the harmonic function $h(z, \mu) = z$ (the unique positive harmonic function that vanishes on the boundary $z = 0$ for the two-dimensional diffusion). Under the h -transform the

conditioned bridge midpoint density is

$$p_h(z, \mu; T/2) \propto h(z, \mu) \cdot p_0(z, \mu; T/2) \propto z \exp\left(-\frac{z^2}{\sigma_z^2 T}\right) \exp\left(-\frac{\mu^2}{\sigma_\mu^2 T}\right). \quad (15)$$

Marginalising over μ (which contributes only a constant) yields

$$p_h(z; T/2) \propto z e^{-z^2/(\sigma_z^2 T)}, \quad (16)$$

which is precisely the **Rayleigh distribution** with scale $\sigma = \sigma_z \sqrt{T}/\sqrt{2}$. The z -factor in the numerator—absent in the scalar case where $h(z) = z$ already gives Rayleigh but the conditioning is one-dimensional—arises here because the second coordinate μ is free to fluctuate, making the effective conditioning softer and shifting probability toward larger z .

This argument is heuristic in the diffusion limit and provides a physical foundation for the Rayleigh observation, but a rigorous Pitman-type theorem for the pre-asymptotic (z, μ_z) process remains an important open problem (Appendix B, Q2).

Physical interpretation of the geometry–amplitude separation. The bridge constraint $z(0) = z(n_s) = 0$ is a global boundary condition that fixes the macroscopic envelope of the trajectory. The resulting parabolic shape $4t(1-t)$ is therefore determined by the endpoint conditions alone and is insensitive to whether the microscopic dynamics are isotropic ($g = 0$) or strongly forward-peaked ($g = 0.95$). In contrast, the amplitude of the excursion is controlled by the statistical structure of the increments: even weak persistence in the direction cosine μ_z inflates the effective step size and raises the scaling exponent above $1/2$. The two anomalous exponents α_∞ and β_D are signatures of this increment structure, not of the shape. More precisely, both exponents measure how the excursion constraint suppresses fluctuations in a 2D Markov process: the z -coordinate is confined to the half-space, but the coupled variable μ_z is free, and it is this freedom that shifts both exponents away from their Brownian-excursion values.

The shift from Rayleigh to Maxwell at $g = 0.9$ has a natural physical explanation rooted in the diffusive-to-ballistic crossover controlled by the transport mean free path $\lambda^* = 1/(1-g)$.

At low g (isotropic or weakly forward scattering), μ_z randomises in approximately one step. The direction cosine decorrelates on a length scale of order $\lambda^* \sim 1$, so within a few steps the walk has lost memory of its initial direction. The effective state space is two-dimensional, (z, μ_z) , with μ_z fluctuating rapidly—and the Doob h -transform argument of Section 4.1 applies directly, giving a Rayleigh marginal.

At $g = 0.9$, however, $\lambda^* = 10$: the photon is nearly forward-directed and sustains its direction for ~ 10 steps before appreciable randomisation occurs. This long ballistic

correlation time means that μ_z is no longer a rapidly fluctuating variable that can be marginalised out cleanly. Instead, the slow evolution of μ_z introduces additional persistent modes into the dynamics, effectively enlarging the state space beyond two dimensions. The bridge constraint then acts on a higher-dimensional process, and the marginal distribution of z shifts toward the Maxwell form (Bessel-3 in 3D).

This picture suggests a g -dependent effective Bessel order $n_{\text{eff}}(g)$ that interpolates continuously from 2 (Rayleigh) at $g \rightarrow 0$ toward 3 (Maxwell) as $g \rightarrow 1$, with λ^* as the natural control parameter. A clean test would be to fit $z(n_s/2)$ to a Bessel distribution of non-integer order at intermediate $g \in \{0.6, 0.7, 0.8\}$ and check whether n_{eff} increases monotonically with λ^* . We identify this as a concrete open prediction of the state-space framework (Appendix B, Q6).

The directional-memory profile of Section 3.6 provides an independent window onto the same (z, μ_z) dynamics. The Milne endpoint $\langle \mu_z(n_s - 1) \rangle \rightarrow -2/3$ is the *microscopic* signature of the boundary condition that the bridge must satisfy: the coupled variable μ_z is not free at the endpoint but is constrained to the Lambertian-backward distribution, exactly as in the emergent-flux problem. The g -independence of this constraint is a direct corollary of the H-function universality (Eq. 11), and the linear ramp from $+g$ to $-2/3$ across n_s steps is the directional analogue of the spatial parabolic profile: a universal shape (linear) with an amplitude that carries the g -dependence.

4.2 Relation between the two anomalous exponents

Two anomalous exponents appear in the data: the mean-amplitude exponent $\alpha_\infty \approx 0.573$ (versus the Brownian prediction 0.5) and the transport mean free path exponent $\beta_D \approx 0.415$ (versus the simple-diffusion prediction 1.0). These are not *a priori* related.

The data reveal an empirical relation:

$$\alpha_\infty + \beta_D \approx 0.573 + 0.415 \approx 0.988 \approx 1. \quad (17)$$

The relation $\alpha_\infty + \beta_D \approx 1$ would hold exactly if both exponents represent complementary deviations from a common reference, with a single 2D geometric correction contributing $+\delta$ to the mean exponent and -2δ to the diffusion-coefficient exponent (from $\text{Var} \sim A^2/n_s$), where $\delta \approx 0.07$. This is an empirical relation awaiting theoretical explanation; no derivation is offered, and we do not speculate on rational values (Appendix B, Q3).

4.3 Why not Brownian excursion, and when might convergence occur?

The isotropic HG walk ($g = 0$) has finite-variance increments, so the unconstrained walk converges to Brownian motion by the central limit theorem. Whether the *conditioned*

walk converges to the Brownian excursion is a separate question that depends on the rate at which the (z, μ_z) coupling becomes negligible.

The local exponent α_{local} for $g = 0$ shows no convergence toward 0.5 through $n_s = 200$ (Fig. 3). The approximate stabilisation near 0.57 over $n_s \sim 60\text{--}200$ could represent either a true asymptotic value or an anomalously slow transient. The median excursion length at $g = 0$ is only 8 steps (Table 3), meaning that the typical paths contributing to the large- n_s statistics are the rare deep ones, which may carry the (z, μ_z) coupling most strongly.

Resolving this question requires simulations at $n_s \sim 500\text{--}5000$ for $g = 0$, which is computationally accessible. We identify this as the most important numerical follow-up (Appendix B, Q1).

From a practical standpoint, however, the range $n_s \leq 200$ already covers the physically relevant regime for radiative transport applications. First-return (first-passage) probabilities decay as $P(L) \sim L^{-3/2}$, so the bulk of the excursion ensemble is concentrated at short-to-moderate path lengths: the median excursion length is only 8 steps at $g = 0$ (Table 3), and fewer than 1% of excursions exceed $n_s = 200$. In tissue-optics applications, backscattered photons typically complete tens to low hundreds of scattering events before re-emerging; path lengths of $n_s \sim 10^3\text{--}10^4$ are physically unrealisable under normal conditions. The pre-asymptotic scaling regime we characterise is therefore not a limitation but the regime of physical relevance: whether convergence to Brownian-excursion behaviour ultimately occurs at astronomically large n_s is mathematically interesting but does not affect the applicability of our results to real photon-transport problems.

5 Conclusions

We have characterised the scaling properties of Henyey-Greenstein bridge paths through systematic Monte Carlo simulation across $g \in [0, 0.95]$ and $n_s \in [4, 200]$. The principal findings are:

1. **Universal parabolic shape:** both mean and variance profiles collapse onto $4t(1-t)$ for all g and n_s .
2. **Diffusive variance with anomalous λ^* scaling:** $\text{Var} \sim D(g)n_s$ with $D(g) \propto (\lambda^*)^{\beta_D}$ ($\beta_D \approx 0.415$) rather than the simple-diffusion prediction $\beta_D = 1$.
3. **Super-diffusive mean:** $A \sim n_s^\alpha$ with $\alpha_\infty \approx 0.57$ for $g = 0$, rising to $\alpha \approx 1.15$ at $g = 0.95$. No convergence to $\alpha = 0.5$ is observed to $n_s = 200$.
4. **Rayleigh (2D-Bessel) midpoint distribution:** $z(n_s/2)$ converges to Rayleigh for $g \leq 0.5$, indicating a two-dimensional Bessel process rather than the 1D half-normal of Brownian-excursion theory.

5. **Robustness:** results are invariant under a fivefold reduction of the bridge tolerance ε and under replacement of the fixed-length criterion by natural first-passage stopping.
6. **Milne endpoint of the directional profile:** the bridge-conditioned mean $\langle \mu_z(j) \rangle$ interpolates linearly from +1 at launch through 0 at midpoint to the g -independent Milne value $-2/3$ at the final step. The endpoint follows from the classical H-function moment identity and provides a microscopic interpretation of the return-to-surface constraint.

All anomalies are attributed to the two-dimensional (z, μ_z) Markovian state space: conditioning a 2D process to remain in a half-plane produces a 2D-Bessel (Rayleigh) marginal rather than the 1D-Bessel (half-normal) expected from scalar-walk theory. The empirical relation $\alpha_\infty + \beta_D \approx 1$ suggests a single underlying geometric correction. A rigorous Pitman-type theorem for the conditioned (z, μ_z) process, and a theoretical prediction for the exponent values, remain important open problems.

The results place HG bridge paths in a broader class of constrained stochastic processes characterised by a *separation between geometry and amplitude scaling*: the excursion shape appears universal across the tested parameter range and is determined by the global boundary conditions, while the amplitude scaling retains memory of the microscopic dynamics. Within the range of parameters studied here ($g \in [0, 0.95]$, $n_s \leq 200$), the HG walk behaves consistently with a 2D-Bessel (Rayleigh) universality class, raising the scaling exponent from $1/2$ to ≈ 0.57 ; whether this persists asymptotically remains the primary open question.

In the radiative-transport context the practical implication is direct: backscattered photons completing exactly n_s scattering events probe tissue at depths scaling as $n_s^{0.57} \approx 0.58$ rather than the diffusive $n_s^{0.5}$, meaning depth-resolved diagnostics that assume Brownian-excursion scaling will systematically underestimate the sampled depth. This statement applies within the idealized single-scattering model studied here; real biological media include absorption, refractive boundaries, and finite geometry, whose effects on the bridge scaling exponent remain to be characterised.

Acknowledgements

This paper is a direct spinoff of an intensive programme of Monte Carlo calculations on first-return statistics in Henyey–Greenstein scattering and their connection to Motzkin polynomials, carried out by one of the authors (C.Z.) [12, 13]. The bridge process, the super-diffusive scaling exponents, and the directional-memory profiles reported here emerged as a byproduct of that foundational numerical work.

The authors also thank the open-source scientific Python ecosystem (NumPy, SciPy, Matplotlib). Portions of the numerical analysis, figure preparation, and manuscript drafting were assisted by Claude (Anthropic).

A Peak Mean Depth Data

Table 2 gives the peak mean depth $A(g, n_s)$ in units of the mean free path. Values for $n_s \leq 40$ are from earlier simulations; extended runs ($n_s = 50$ – 200) are for $g = 0.0$ and $g = 0.1$ from the present study.

Table 2: Peak mean depth $A(g, n_s)$ [mean free paths].

$g \backslash n_s$	4	6	8	10	15	20	25	30	40
0.00	0.616	0.861	1.098	1.276	1.735	2.117	2.437	2.759	3.353
0.10	0.620	0.905	1.145	1.357	1.823	2.237	2.573	2.900	3.489
0.20	0.644	0.947	1.217	1.443	1.937	2.358	2.725	3.081	3.710
0.30	0.671	0.994	1.292	1.515	2.064	2.460	2.899	3.278	3.921
0.40	0.671	1.025	1.356	1.620	2.190	2.632	3.097	3.500	4.194
0.50	0.680	1.081	1.423	1.739	2.356	2.869	3.339	3.751	4.503
0.60	0.679	1.108	1.489	1.844	2.569	3.167	3.612	4.155	4.962
0.70	0.669	1.122	1.542	1.946	2.798	3.510	4.142	4.646	5.548
0.80	0.658	1.118	1.563	2.030	3.088	3.983	4.731	5.443	6.621
0.90	0.638	1.092	1.539	2.015	3.210	4.378	5.447	6.430	8.236
0.95	0.643	1.051	1.514	1.976	3.217	4.375	5.575	6.725	9.015

Extended runs: $g = 0.0$: (50, 3.91), (60, 4.23), (80, 5.09), (100, 5.75), (150, 7.24), (200, 8.58).
 $g = 0.1$: (50, 4.03), (60, 4.45), (80, 5.31), (100, 5.99), (150, 7.62), (200, 8.94).

Table 3: Scaling exponent α from natural first-passage excursions (power-law fit over $L = 10$ – 300 , $N_T = 2 \times 10^6$ walkers each).

g	α	C	Median L
0.0	0.614	0.504	8
0.3	0.630	0.543	11
0.5	0.646	0.577	15
0.7	0.675	0.610	23
0.9	0.755	0.605	55

B Open Questions

Q1 — Asymptotic exponent. Is $\alpha_\infty \approx 0.57$ a permanent feature of the conditioned (z, μ_z) process, or an anomalously slow pre-asymptotic transient? Simulations at $n_s = 500$ –

5000 for $g = 0$ are computationally accessible and could determine whether the local exponent continues to drift toward 0.5 or stabilises.

Q2 — Rigorous 2D-Bessel theorem. Why does the midpoint distribution converge to Rayleigh (2D) rather than half-normal (1D)? The (z, μ_z) state-space interpretation provides a qualitative answer; a rigorous Pitman-type theorem for conditioned 2D Markov processes would be of independent mathematical interest. Does the effective Bessel order depend continuously on g , shifting from 1 toward $3/2$ as $g \rightarrow 1$?

Q3 — Exponent relation. Is the empirical relation $\alpha_\infty + \beta_D \approx 1$ exact? If so, is the correction $\delta \approx 1/12$ derivable from a symmetry or dimensional argument in the (z, μ_z) space?

Q4 — Diffusion coefficient exponent. Why is $\beta_D \approx 0.415$ rather than 1.0? Is there a renormalisation-group argument relating the excursion constraint to the effective diffusivity scaling with λ^* ?

Q5 — Origin of the universal parabolic profile. The collapse of normalised mean and variance profiles onto $4t(1-t)$ holds for all g and n_s tested. The same parabola describes the mean profile of a Brownian bridge (pinned at both ends, no positivity constraint), suggesting the shape is determined entirely by the endpoint boundary conditions and is independent of the internal dynamics. A clean way to state this: for *any* bridge process whose increments have finite variance, the normalised mean profile converges to $4t(1-t)$ as $n_s \rightarrow \infty$. This would follow from the fact that the bridge mean profile is $\langle z(j) \rangle = j(n_s - j)\langle \Delta z \rangle / n_s$ for processes with stationary increments, which normalises exactly to $4t(1-t)$ up to a constant. A formal proof for non-stationary increment processes (such as the HG walk with $g > 0$) would be of independent interest.

Q6 — g -dependent effective Bessel order. The midpoint distribution shifts from Rayleigh (Bessel-2D, $g \leq 0.5$) toward Maxwell (Bessel-3D, $g = 0.9$), consistent with the ballistic correlation length $\lambda^* = 1/(1-g)$ enlarging the effective state-space dimensionality. A concrete test: fit $z(n_s/2)$ to a Bessel distribution of non-integer order n_{eff} at intermediate $g \in \{0.6, 0.7, 0.8\}$ and determine whether $n_{\text{eff}}(g)$ increases monotonically with λ^* . If confirmed, this would establish λ^* as the natural control parameter governing the diffusive-to-ballistic crossover in the conditioned process.

Q7 — Directional memory profile: remaining data. Figure 8 presents MC data for $\mu_0 \in \{0.25, 0.50, 0.75, 1.00\}$ at $g = 0.5$, $n_s = 40$, confirming universality of the zero-crossing and Milne endpoint with respect to μ_0 . Outstanding items are: (i) MC scoring of

$\langle \mu_z(j) \rangle_{\text{bridge}}$ for $g \in \{0.3, 0.7, 0.9\}$ at $n_s = 30$, to validate Eq. (12) across the full g -range; (ii) early-step values $j = 0, 1, 2$ for all g , including the bridge-conditioned $\langle \mu_z(1) \rangle_{\text{bridge}}$, which is expected to exceed the free-walk value g due to the forward-step selection imposed by the bridge constraint; and (iii) a larger- n_s overlay (e.g. $n_s = 100$, $g = 0.5$) to confirm n_s -independence of the normalised profile.

References

- [1] R. T. Durrett, D. L. Iglehart, and D. R. Miller, “Weak convergence to Brownian meander and Brownian excursion,” *Ann. Probab.* **5**(1), 117–129 (1977).
- [2] R. T. Durrett and D. L. Iglehart, “Functionals of Brownian meander and Brownian excursion,” *Ann. Probab.* **5**(1), 130–135 (1977).
- [3] D. L. Iglehart, “Functional central limit theorems for random walks conditioned to stay positive,” *Ann. Probab.* **2**(4), 608–619 (1974).
- [4] L. G. Henyey and J. L. Greenstein, “Diffuse radiation in the galaxy,” *Astrophys. J.* **93**, 70–83 (1941).
- [5] L. Wang, S. L. Jacques, and L. Zheng, “MCML—Monte Carlo modeling of light transport in multi-layered tissues,” *Comput. Methods Programs Biomed.* **47**(2), 131–146 (1995).
- [6] A. Ishimaru, *Wave Propagation and Scattering in Random Media*, Vols. 1–2 (Academic Press, New York, 1978).
- [7] J. W. Pitman, “One-dimensional Brownian motion and the three-dimensional Bessel process,” *Adv. Appl. Probab.* **7**(3), 511–526 (1975).
- [8] L. Chaumont and R. A. Doney, “On Lévy processes conditioned to stay positive,” *Electron. J. Probab.* **10**, 948–961 (2005).
- [9] L. Chaumont and R. A. Doney, “Corrections to ‘On Lévy processes conditioned to stay positive,’” *Electron. J. Probab.* **13**, 1–4 (2008).
- [10] D. Denisov, A. Tarasov, and V. Wachtel, “Asymptotic expansions for random walks conditioned to stay positive,” *Electron. J. Probab.* **31**, paper 24 (2026). [arXiv:2401.09929]
- [11] L. C. G. Rogers and J. W. Pitman, “Markov functions,” *Ann. Probab.* **9**(4), 573–582 (1981).

- [12] C. Zeller and R. Cordery, “First-return statistics in bounded radiative transport: A Motzkin polynomial framework,” arXiv:2512.13986 (2025).
- [13] C. Zeller and R. Cordery, “First-return statistics in Henyey-Greenstein scattering: Colored Motzkin polynomials and the Cauchy kernel,” arXiv:2601.00173 (2026).
- [14] S. Goldstein, “On diffusion by discontinuous movements and on the telegraph equation,” *Q. J. Mech. Appl. Math.* **4**(2), 129–156 (1951).
- [15] M. Kac, “Random walk and the theory of Brownian motion,” *Am. Math. Monthly* **54**(7), 369–391 (1947).
- [16] S. Chandrasekhar, *Radiative Transfer* (Dover Publications, New York, 1960).
- [17] K. M. Case and P. F. Zweifel, *Linear Transport Theory* (Addison-Wesley, Reading MA, 1967).